Available online at www.sciencedirect.com
SCIENCE DIRECT®
Journal of Molecular Structure 692 (2004) 91–106
Journal of MOLECULAR STRUCTURE
www.elsevier.com/locate/molstruc

β-Nitrostyrene derivatives—a conformational study by combined Raman spectroscopy and ab initio MO calculations

R. Calheiros[a,b], N. Milhazes[c,d], F. Borges[c], M.P.M. Marques[a,b,*]

[a]*Research Unit 'Molecular Physical-Chemistry', University of Coimbra, 3001-401 Coimbra, Portugal*
[b]*Department of Biochemistry, Faculty of Sciences and Technology, University Coimbra, Ap. 3126, 3001-401 Coimbra, Portugal*
[c]*Department of CEQUP/Chemistry, Faculty of Sciences and Technology, University of Porto, 4169-007 Porto, Portugal*
[d]*Superior Institute of Health Sciences-North, 4580 Paredes, Portugal*

Received 11 November 2003; revised 9 January 2004; accepted 12 January 2004

Abstract

A complete conformational analysis of β-nitrostyrene and β-methyl-β-nitrostyrene derivatives was carried out by Raman spectroscopy coupled to ab initio MO calculations. Apart from the optimised geometrical parameters of the most stable conformers of the molecules under study, the corresponding harmonic vibrational frequencies were calculated, as well as potential-energy profiles for several internal rotations within the molecules. At the light of these results, a complete assignment of the Raman spectra of the solid samples was performed. The conformational behaviour of this kind of systems was found to be mainly determined by the stabilising effect of π-electron delocalisation.

Keywords: β-nitrostyrene; β-methyl-β-nitrostyrene; Raman spectroscopy; Ab initio calculations; Conformational analysis

1. Introduction

β-Nitrostyrenes and their derivatives are important starting materials for the synthesis of a variety of useful building blocks, such as nitroalkanes, amines, ketoximes, hydroxylamines and aldoximes [1,2]. Moreover, conjugated nitroalkenes are exceptionally good Michael acceptors, namely towards organometallic reagents [3] and vitamin C [4]. Nitrostyrenes are activated alkenes displaying an electron-withdrawing NO_2 group, which have been shown to predominate in the ground state *E* (*trans*) configuration of the nitro and phenyl groups relative to the carbon chain double bond [5].

Apart from their well recognised antimicrobial and antifungal activities [6], nitrostyrene derivatives have lately been shown to constitute a novel class of chemical compounds with good potential for further development as promising anticancer drugs [7,8]. In fact, some reported studies [8] propose a nitrovinyl side chain attached to an aromatic ring as the pharmacophore structure of a new group of pro-apoptotic agents.

Once the biological activity of this type of compounds is thought to be strongly dependent on their structural characteristics—similarly to what has been found for phenolic acids and phenolic ester analogues [9]—a series of ring-substituted nitrostyrenes was synthesised in our lab, and screened for their in vitro and in vivo antiproliferative and cytotoxic properties (both in human cancer cells and in live mice).

The present work reports the conformational analysis of β-nitrostyrene derivatives, as well as of some of their analogues and synthetic precursors, by Raman spectroscopy coupled to ab initio MO methods (at the DFT level). The compounds studied were: 1,2-dihydroxybenzene (catechol, CAT), 3,4-dihydroxybenzaldehyde (3,4-OH-BA), styrene (S), β-methyl-styrene (MeS), β-nitrostyrene (NS), β-methyl-β-nitrostyrene (MeNS), 3,4-dihydroxy-β-nitrostyrene (3,4-OH-NS) and 3,4-dihydroxy-β-methyl-β-nitrostyrene (3,4-OH-MeNS) (Fig. 1).

* Corresponding author. Address: Department of Biochemistry, Faculty of Sciences and Technology, University Coimbra, Ap. 3126, 3001-401 Coimbra, Portugal. Tel.: +351-239854462; fax: +351-239826541.
E-mail address: pmc@ci.uc.pt (M.P.M. Marques).

0022-2860/$ - see front matter © 2004 Elsevier B.V. All rights reserved.
doi:10.1016/j.molstruc.2004.01.012

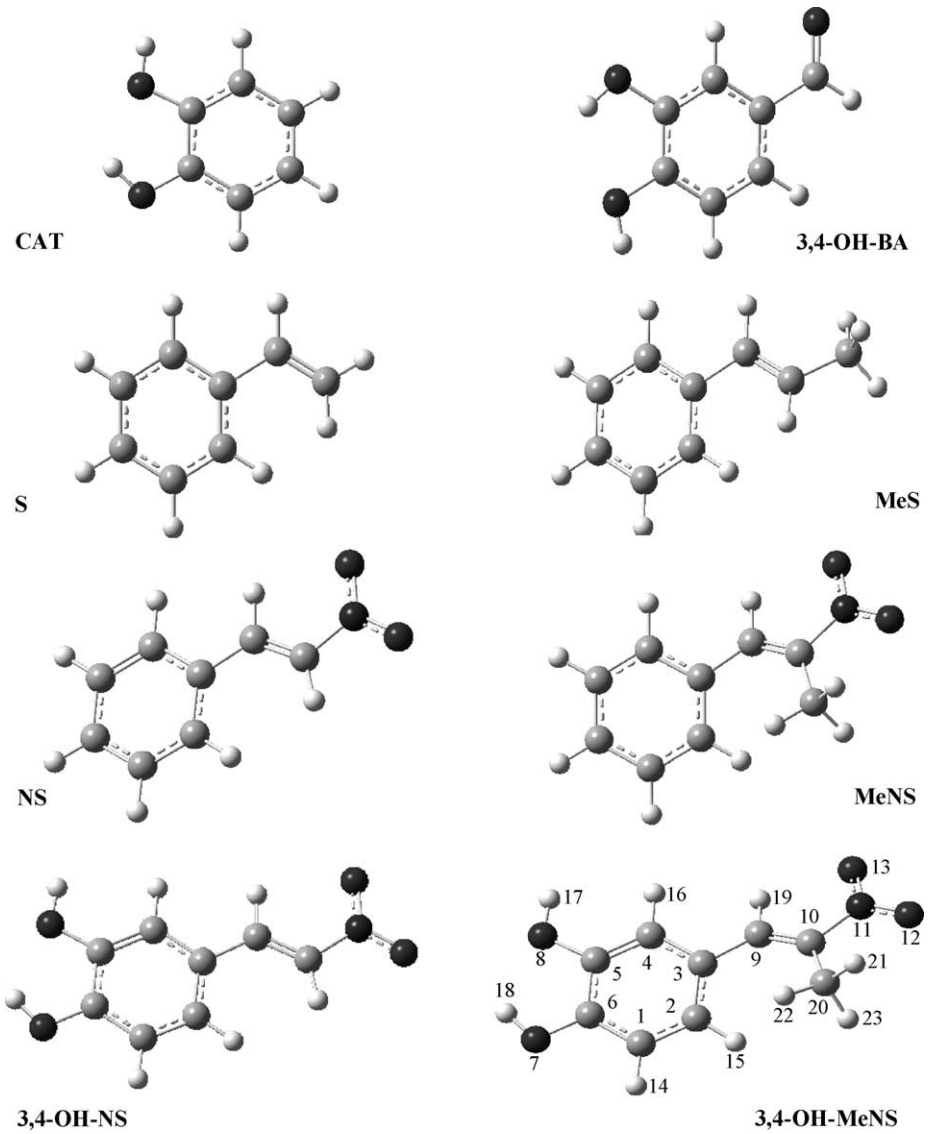

Fig. 1. Schematic representation of the β-nitrostyrene derivatives, and their analogues, studied in the present work. For NS, MeNS, 3,4-OH-NS and 3,4-OH-MeNS, the calculated (B3LYP/6-31G**) lowest energy conformers are displayed (the atom numbering is included, and is applicable to all the compounds studied, irrespective of the type of atom).

2. Experimental

2.1. Synthesis

The synthetic procedure was adapted from Parker et al. [10] with slight modifications. A mixture of the benzaldehyde (5.0 g), with the corresponding substitution pattern, and ammonium acetate (0.5 g) was dissolved in nitroethane (50 ml)—for the β-methyl-β-nitrostyrene derivatives—or in nitromethane (50 ml)—for the β-nitrostyrene derivatives—and refluxed for 5 h. After cooling to room temperature the reaction mixtures were partially evaporated in a rotary evaporator, diluted with diethyl ether and washed twice with water. The organic layer was dried over anhydrous magnesium sulphate, filtered and concentrated. The remaining residues were recrystallised from diethylether/petroleum ether. The synthesised compounds were identified by both NMR and electron impact mass spectra (EI-MS).

β-Methyl-β-nitrostyrene (MeNS). Yield 6.38 g, 83%; ^{1}H NMR δ: 2.38 (3H, s, CH_3), 7.47–7.51 (3H, m, Ar*H*), 7.56–7.59 (2H, m, Ar*H*), 8.08 (1H, s, H(α)); ^{13}C NMR δ: *13.9* CH_3, *129.0* (2 × *C*HAr), 129.2 C(β), *130.3* (2 × *C*HAr), *133.2 C*HAr, *147.7* C(1); EI-MS *m/z* (%): 163 ($M^{+\cdot}$, 16), 146 (15), 115 (100), 105 (99), 91 (56), 77 (51), 65 (15); m.p. 58–61 °C.

3,4-Dihydroxy-β-nitrostyrene (3,4-OH-NS). Yield 2.26 g, 34%; ^{1}H NMR δ: 6.81 (1H, d, $J = 8.7$, H(5)), 7.19 (1H, d, $J = 2.2$, H(2)), 7.20 (1H, dd, $J = 8.0$; 2.2, H(6)), 7.93 (1H, d, $J = 13.5$, H(α)), 7.98 (1H, d, $J = 13.5$, H(β)),

9.70 (2H, *brs*, O*H*); ^{13}C NMR δ: *116.0 C*HAr, *116.4 C*HAr, 121.5 C(1), *123.8 C*HAr, *134.6* C(α), *140.4* C(β), 145.8 C(3), 150.5 C(4); EI-MS *m/z* (%): 181 ($M^{+\cdot}$, 100), 134 (85), 89 (47), 77 (31), 63 (24); m.p. 148–151 °C.

3,4-Dihydroxy-β-methyl-β-nitrostyrene (3,4-OH-MeNS). Yield 2.55 g, 35%; ^{1}H NMR δ: 2.40 (3H, s, C*H*$_3$) 6.85 (1H, d, $J = 8.2$, H(5)), 6.97 (1H, dd, $J = 8.3$; 2.0, H(6)), 7.05 (1H, d, $J = 2.0$, H(2)), 7.96 (1H, s, H(α)), 9.58 (2H, *brs*, O*H*); ^{13}C NMR δ: 14.0 *C*H$_3$, *116.0 C*HAr, *117.5 C*HAr, 123.1 C(1), *124.0 C*HAr, *134.2* C(α), *144.3*C(β), 145.6 C(3), 148.4 C(4); EI-MS *m/z* (%): 195 ($M^{+\cdot}$, 99), 148 (69), 138 (24), 119 (16), 110 (17), 103 (100), 91 (40), 83 (23), 77 (53), 65 (23), 55 (17); m.p. 140–141 °C.

2.2. Apparatus

^{1}H and ^{13}C NMR data were acquired, at room temperature, on a Brüker AMX 300 spectrometer operating at 300.13 and 75.47 MHz, respectively. Dimethylsulfoxide-d_6 was used as a solvent; chemical shifts are expressed in δ (ppm) values relative to tetramethylsilane (TMS) as internal reference; coupling constants (*J*) are given in Hertz. Assignments were also made from distortionless enhancement by polarization transfer (DEPT) (see italicised values). EI-MS were carried out on a VG AutoSpec instrument; the data are reported as *m/z* (% of relative intensity of the most important fragments). Melting points were obtained on a Köfler microscope (Reichert Thermovar) and are uncorrected.

2.3. Ab initio MO calculations

The ab initio calculations—full geometry optimisation and calculation of the harmonic vibrational frequencies—were performed using the GAUSSIAN 98W program [11], within the Density Functional Theory (DFT) approach, in order to properly account for the electron correlation effects (particularly important in this kind of systems). The widely employed hybrid method denoted by B3LYP [12–17], which includes a mixture of HF and DFT exchange terms and the gradient-corrected correlation functional of Lee et al. [18,19], as proposed and parameterised by Becke [20,21], was used, along with the double-zeta split valence basis sets 6-31G* and 6-31G** [22,23].

Molecular geometries were fully optimised by the Berny algorithm, using redundant internal coordinates [24]: the bond lengths to within ca. 0.1 pm and the bond angles to within ca. 0.1°. The final root-mean-square (rms) gradients were always less than 3×10^{-4} hartree bohr^{-1} or hartree rad^{-1}. No geometrical constraints were imposed on the molecules under study. The 6-31G** basis set was used for all geometry optimisations, while for most of the rotational energy barrier calculations the smaller basis set 6-31G* was found to yield good results. All frequency calculations were run at the B3LYP/6-31G** level and wavenumbers above 400 cm^{-1} were scaled [25] before comparing them with reported experimental data.

Quantitative potential-energy profiles for rotation around different bonds within the molecule were obtained, by scanning the corresponding dihedrals and using least-squares fitted Fourier-type functions of a dihedral angle, τ [26,27]:

$$P = \sum_{n=1}^{3} \frac{1}{2} P_n [1 - \cos(n\tau)] + \sum_{m=1}^{2} \frac{1}{2} P'_m \sin(m\tau) \quad (1)$$

The parameters P_n and P'_m correspond to potential-energy (V_n and V_m terms), bond-distance or bond-angle differences relative to a reference value. According to the symmetry of the nitrostyrene molecules presently studied, namely the methyl substituted ones, both cosine and sine terms were considered in the fitting of the experimental data.

2.4. Spectroscopic methods

The Raman spectra were obtained, at room temperature, on a triple monochromator Jobin-Yvon T64000 Raman system (0.640 m, *f*/7.5) with holographic gratings of 1800 grooves mm^{-1}. The detection system was a non-intensified Charge Coupled Device (CCD). The entrance slit was set to 100 μm and the slit between the premonochromator and the spectrograph was opened to 14.0 mm. The 514.5 nm line of an Ar^+ laser (Coherent, model Innova 300) was used as excitation radiation, providing 5–100 mW at the sample position. Samples (pure solids) were sealed in Kimax glass capillary tubes of 0.8 mm inner diameter. Under the above mentioned conditions, the error in wavenumbers was estimated to be within 1 cm^{-1}.

In some cases, the Ar^+ laser 514.5 nm excitation line led to quite strong fluorescence backgrounds, which were avoided by lowering the laser power or, when this was not enough, by using a 1064 nm line provided by a Nd:YAG laser (FT-Raman experiments).

Fourier transform Raman spectra were recorded on a RFS 100/S Bruker spectrometer, with a 180° geometry, equipped with an InGaAs detector. Near-infrared excitation was provided by the 1064 nm line of a Nd:YAG laser (Coherent, model Compass-1064/500N). A laser power of 200 mW at the sample position was used in all cases, and resolution was set to 2 cm^{-1}.

FT-IR data was collected (in KBr pellets) on a MATSON 7000 spectrometer, operating in the 400–4000 cm^{-1} range, using a 2 cm^{-1} resolution.

2.5. Chemicals

trans-β-Nitrostyrene, 1,2-dihydroxybenzene, 3,4-dihydroxybenzaldehyde, styrene, *trans*-β-methylstyrene, ammonium acetate, nitroethane and nitromethane were purchased from Sigma-Aldrich Química S.A. (Sintra, Portugal). All other reagents and solvents were *pro-analysis* grade, purchased from Merck (Lisbon, Portugal).

3. Results and discussion

3.1. Ab initio MO calculations

A complete geometry optimisation was carried out for some of the nitrostyrenes under study, namely: β-nitrostyrene (NS), β-methyl-β-nitrostyrene (MeNS), 3,4-dihydroxy-β-nitrostyrene (3,4-OH-NS) and 3,4-dihydroxy-β-methyl-β-nitrostyrene (3,4-OH-MeNS). The effect of several structural parameters on the overall stability of these molecules was investigated: (i) orientation of the phenolic hydroxyls, relative to the ring—dihedrals ($H_{17}O_8C_5C_4$) and ($H_{18}O_7C_6C_5$) equal to 0 or 180° (Fig. 1); (ii) relative orientation of the aromatic ring and the NO_2 group relative to the $C_9{=}C_{10}$ bond—($C_3C_9C_{10}N_{11}$) dihedral equal to 0 or 180°, defining a *Z* or *E* configuration, respectively; (iii) position of the methyl

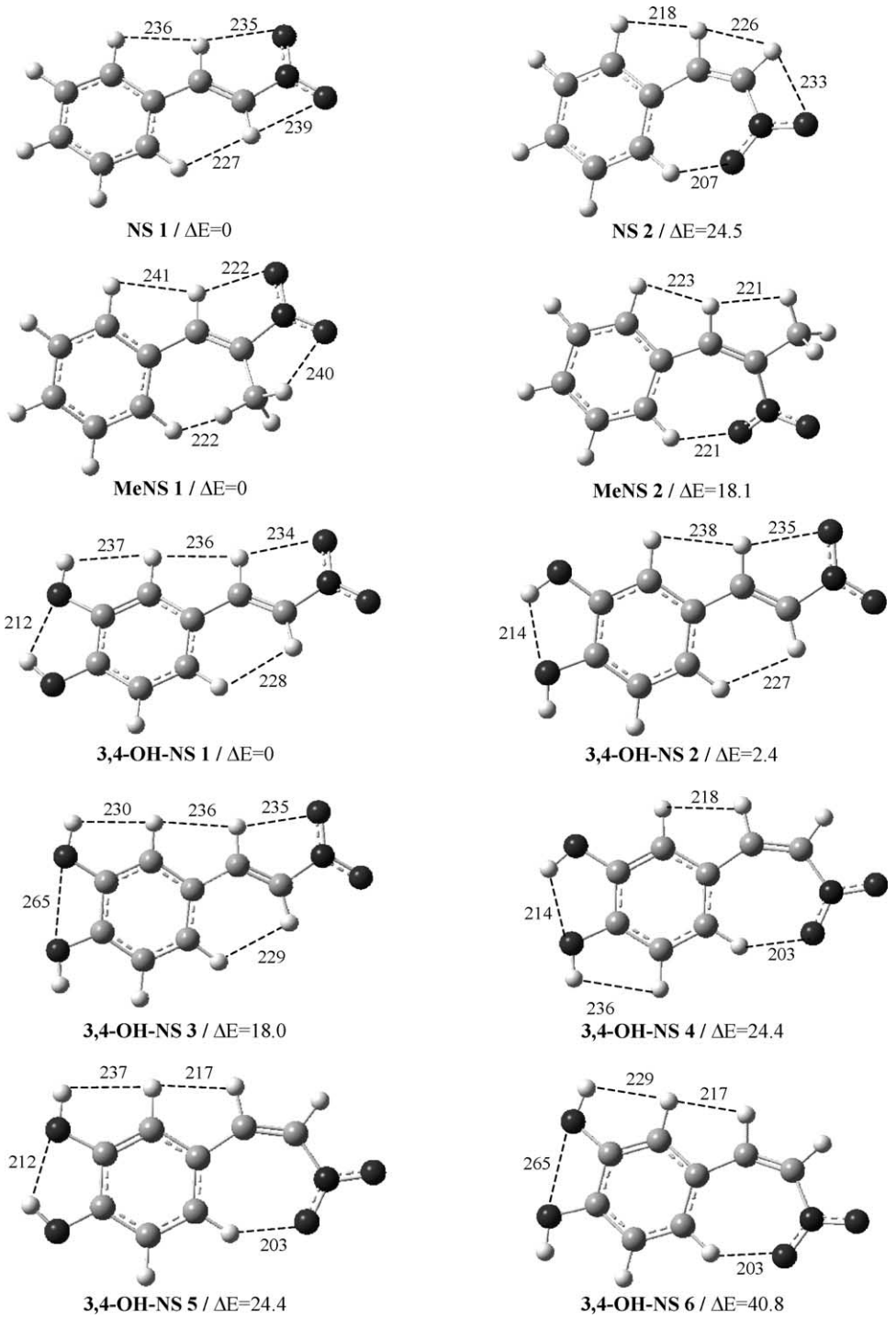

Fig. 2. Schematic representation of the calculated (B3LYP/6-31G**) conformers for β-nitrostyrene (NS), β-methyl-β-nitrostyrene (MeNS) and 3,4-dihydroxy-β-nitrostyrene (3,4-OH-NS) (displaying intramolecular hydrogen bonds—distances in pm. Relative energies are in kJ mol^{-1}).

Table 1
Optimised geometries for the most stable conformers of NS, MeNS and 3,4-OH-NS (B3LYP/6-31G** level of calculation)

μ (D)[a]	NS 1 5.8	MeNS **1** 5.2	3,4-OH-NS 1 6.2
Bond lengths (pm)			
C_1-C_2[b]	139.0	139.3	138.9
C_2-C_3	140.9	140.8	140.8
C_3-C_4	140.7	140.9	141.2
C_4-C_5	139.3	139.1	138.4
C_5-C_6	139.5	139.6	140.8
C_6-C_1	139.9	139.6	139.6
C_3-C_9	146.0	146.4	145.3
C_9-C_{10}	134.0	134.6	134.3
$C_{10}-C_{20}$		149.6	
C_5-O_8			137.4
C_6-O_7			135.4
$C_{10}-N_{11}$	145.1	148.4	144.7
$N_{11}-O_{12}$	123.5	123.3	123.5
$N_{11}-O_{13}$	123.3	123.2	123.5
O_8-H_{17}			0.96
O_7-H_{18}			0.97
C_1-H_{14}	108.6	108.6	108.4
C_2-H_{15}	108.5	108.4	108.4
C_4-H_{16}	108.6	108.6	108.8
C_5-H_8	108.5	108.6	
C_6-H_7	108.6	108.6	
C_9-H_{19}	108.7	108.6	108.7
$C_{10}-H_{20}$	108.0		108.0
$C_{20}-H_{21}$		109.1	
$C_{20}-H_{22}$		109.1	
$C_{20}-H_{23}$		109.6	
Bond angles (°)			
$C_2-C_3-C_4$	118.5	118.2	118.3
$C_2-C_3-C_9$	123.2	124.1	123.5
$C_3-C_9-C_{10}$	127.1	129.1	127.4
$C_9-C_{10}-C_{20}$		130.1	
$C_6-C_5-O_8$			114.6
$C_9-C_{10}-N_{11}$	120.5	115.7	120.3
$C_{10}-N_{11}-O_{12}$	115.7	116.4	115.8
$O_{12}-N_{11}-O_{13}$	124.8	124.0	124.6
$C_5-O_8-H_{17}$			110.3
$C_{10}-C_9-H_{19}$	115.9	115.0	115.5
$C_9-C_{10}-H_{20}$	127.8		127.7
$C_{10}-C_{20}-H_{21}$		110.1	
$C_{10}-C_{20}-H_{22}$		110.1	
$H_{21}-C_{20}-H_{22}$		109.2	
$H_{21}-C_{20}-H_{23}$		106.7	
Dihedral angles (°)			
$C_3-C_4-C_5-C_6$	0.0	−1.3	0.0
$C_5-C_4-C_3-C_9$	0.0	−179.7	180.0
$C_4-C_3-C_9-C_{10}$	180.0	152.3	−180.0
$C_3-C_9-C_{10}-C_{20}$		−3.9	
$C_3-C_9-C_{10}-N_{11}$	180.0	177.8	180.0
$C_9-C_{10}-N_{11}-O_{12}$	180.0	−177.5	−180.0
$C_9-C_{10}-N_{11}-O_{13}$	0.0	2.0	0.0
$C_4-C_5-O_8-H_{17}$			0.0
$C_5-C_6-O_7-H_{18}$			0.0
$C_3-C_4-C_5-H_8$	−180.0	179.2	
$C_4-C_5-C_6-H_7$	180.0	−179.4	
$C_5-C_6-C_1-H_{14}$	180.0	−178.4	180.0
$C_6-C_1-C_2-H_{15}$	180.0	−177.6	180.0
$C_2-C_3-C_4-H_{16}$	180.0	−178.5	180.0
$C_2-C_3-C_9-H_{19}$	−180.0	151.8	−180.0
$C_3-C_9-C_{10}-H_{20}$	0.0		0.0
$C_9-C_{10}-C_{20}-H_{21}$		−137.4	
$C_9-C_{10}-C_{20}-H_{22}$		−16.9	

[a] $1D = 1/3 \times 10^{-2}$ cm.
[b] Atoms are numbered according to Fig. 1; the same atom numbering is applicable to all the compounds studied, irrespective of the type of atom.

group relative to the ring OH's—dihedral ($C_{10}C_9C_3C_4$) either 0 or 180°. The conformational behaviour of this kind of compounds is mainly determined by electronic effects, as well as by the possibility of occurrence of (C)H···O intramolecular hydrogen bonds, which are medium strength, directional interactions (with a preference for linearity), long known to be relevant for the overall stability of numerous systems [28].

Two stable conformations were calculated for both NS and MeNS, while six were obtained for the dihydroxylated analogue 3,4-OH-NS, only one of these, in each case, being significantly populated at room temperature (Fig. 2). All the conformers were found to display a planar or quasi-planar geometry, differing in the configuration of the phenyl and NO_2 groups relative to the linear chain double bond—either *E* or *Z*—and in the orientation of the ring hydroxyls. The *E* conformers with identical orientations of the ring OH's were determined to be the lowest energy ones (Table 1).

For 3,4-OH-MeNS, in turn, ten different conformers were calculated (Figs. 3 and 4), the most stable ones also having an *E* orientation of the aromatic ring and the terminal nitro group relative to the $C_9{=}C_{10}$ bond ($(C_3C_9C_{10}N_{11}) = 180°/(C_{20}C_{10}C_9C_3) = 0°$), along with an identical orientation of both OH ring substituents—conformers **1** ($\Delta E = 0$), **2** ($\Delta E = 0.6$ kJ mol^{-1}) and **3** ($\Delta E = 1.5$ kJ mol^{-1})—with populations at room temperature of 43, 34 and 23%, respectively (Table 2). Actually, the large energy difference between conformations **2** and **4** ($\Delta E = 13.6$ kJ mol^{-1}) is due solely to the change in the ($C_3C_9C_{10}N_{11}$) dihedral angle from 180 to 0° (Fig. 3). In fact, despite the small $O_{13}\cdots H_{16}$(C) interatomic distance (201 pm, Fig. 3) in 3,4-OH-MeNS **4**, leading to the formation of a 7-membered intramolecular ring, the $H_{15}\cdots H_{19}$ and $H_{23}\cdots H_{19}$ steric hindrance (H···H distances of 216 and 214 pm, respectively) overrules that stabilising factor. As expected, no stable geometry was obtained when both ring hydroxyl groups are directed towards each other. However, three conformers were found for opposite orientations of the phenolic OH's—3,4-OH-MeNS **5** ($\Delta E = 18.1$ kJ mol^{-1}), **9** ($\Delta E = 33.9$ kJ mol^{-1}) and **10** ($\Delta E = 38.7$ kJ mol^{-1})—these being the less stable ones (e.g. 3,4-OH-MeNS **5** vs. 3,4-OH-MeNS **1** and **2**, Fig. 3). For such an arrangement of the OH groups, a ($C_3C_9C_{10}C_{20}$)

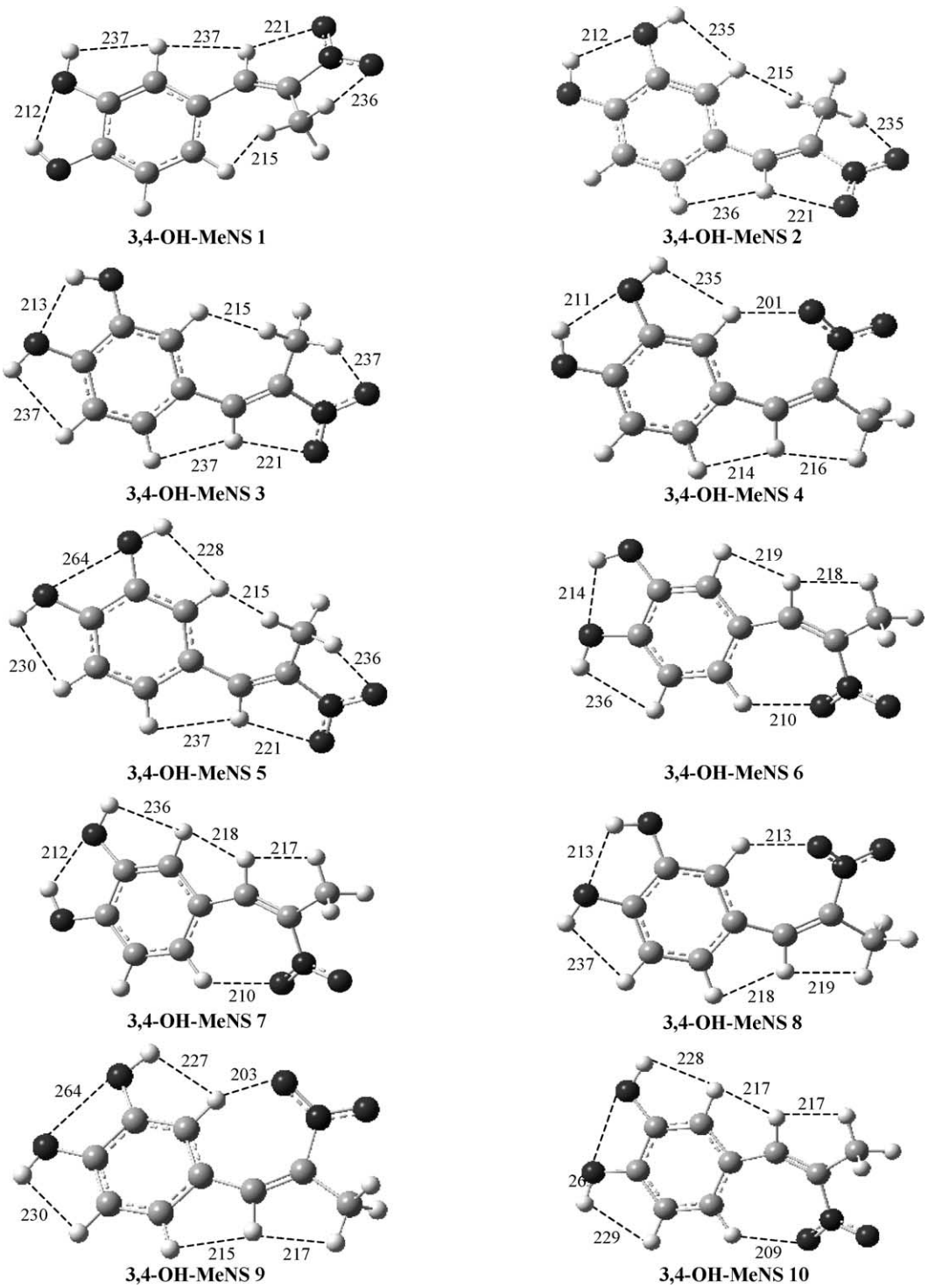

Fig. 3. Schematic representation of the calculated (B3LYP/6-31G**) lowest energy conformers for 3,4-OH-MeNS (displaying intramolecular hydrogen bonds—distances in pm).

dihedral equal to 0° yielded more stable geometries than ($C_3C_9C_{10}C_{20}$) = 180°—3,4-OH-MeNS **5** vs. **9** (Figs. 3 and 4)—on account of the steric repulsion between H_{15} and H_{19} ($H_{15}\cdots H_{19}$ of 215 pm), and H_{19} and H_{22} ($H_{15}\cdots H_{19}$ of 217 pm), which is present in conformer **9**. In contrast, whenever the two ring hydroxyls display the same orientation an energetically favoured geometry results, probably due to the formation of intramolecular hydrogen interactions between O_8 and H_{18}, or O_7 and H_{17} ($O\cdots H$ distances between 211 and 214 pm, Fig. 3).

Moreover, for a ($C_3C_9C_{10}N_{11}$) dihedral equal to 180°, a *syn* orientation of the NO_2 group relative to the OH ring

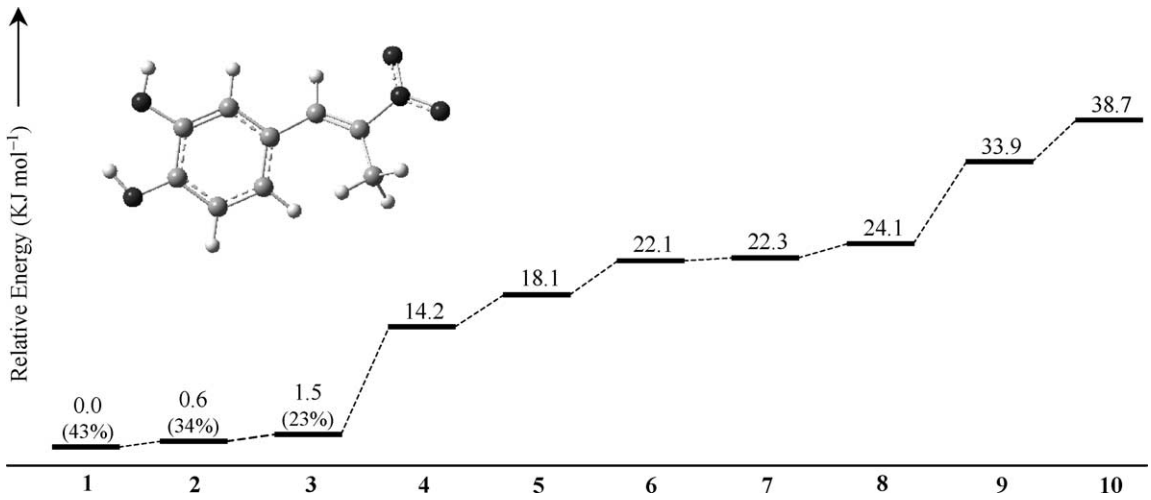

Fig. 4. Schematic representation of the relative conformational energies (and populations, at 25 °C) of the calculated (B3LYP/6-31G**) conformers for 3,4-OH-MeNS.

substituents is energetically favoured, as it allows a more effective electron delocalisation—3,4-OH-MeNS **1** ($\Delta E = 0$) vs. **2** ($\Delta E = 0.6$ kJ mol^{-1}). Also, the zero ($C_4C_3C_9C_{10}$) dihedral in conformation **2** leads to a serious steric hindrance between atoms H_{22} and H_{16}, and H_{19} and H_{15} ($H_{22}\cdots H_{16}$ and $H_{19}\cdots H_{15}$ distances equal to 215 and 236 pm, respectively, Fig. 3). As to the position of the methyl group, it was verified that the geometries displaying a ($C_4C_3C_9C_{10}$) dihedral angle of 0°, a *syn* orientation relative to the ring hydroxyls is favoured (3,4-OH-MeNS **2** ($\Delta E = 0.6$ kJ mol^{-1}) vs. **3** ($\Delta E = 1.5$ kJ mol^{-1}), Fig. 3).

Conformer 3,4-OH-MeNS **10** (($C_4C_3C_9C_{10}$) = 180°) was found to be highly unfavoured relative to 3,4-OH-MeNS **5** (($C_4C_3C_9C_{10}$) = 0°), due to the formation of a medium strength intramolecular H-bond between O_{12} and H_{23} in the latter ($O\cdots H$ distance of 236 pm, Fig. 3), which can not occur in the former ($O\cdots H$ distance of 257 pm).

Although both hydroxyl groups were found to be coplanar with the aromatic ring in all conformers calculated for 3,4-OH-MeNS, the remaining part of the molecule deviates from planarity—($C_2C_3C_9C_{10}$) ca. 23°, ($C_{20}C_{10}C_9C_3$) ca. 4° and ($O_{12}N_{11}C_{10}C_9$) ca. 2°—the most stable geometries displaying one of the methyl hydrogens approaching an oxygen from the NO_2 group, which allows a medium strength H-bond to be formed ($O\cdots H$ distances between 235 and 237 pm, Fig. 3), as well as a minimisation of the H−H steric repulsions.

Rotational isomerism was also investigated for the methyl-nitrostyrene 3,4-OH- -MeNS, by scanning particular dihedral angles—($O_{12}N_{11}C_{10}C_9$), ($H_{22}C_{20}C_{10}N_{11}$) and ($C_{10}C_9C_3C_4$)—which define, respectively, the internal rotation of the nitro and methyl groups, and the orientation of the pendant carbon chain relative to the aromatic ring.

The value of the ($O_{12}N_{11}C_{10}C_9$) dihedral determines the rotation around the $C_{10}-N_{11}$ bond, i.e. the orientation of the NO_2 terminal relative to both the aromatic ring and the double bond in the carbon side chain of the 3,4-OH-MeNS molecule. The analysis of the Fourier components of the corresponding potential-energy variation (Fig. 5) manifests the preference for a planar geometry of the nitro group, once the cosine term in 90° is clearly destabilising—$V_2^{90^\circ} = 30.2$ kJ mol^{-1}—as compared to the 60 and 180° contributions—$V_1^{180^\circ}$ and $V_3^{60^\circ}$ equal to -1.2 kJ mol^{-1}—e.g. geometries 3,4-OH-MeNS **1**, ($O_{12}N_{11}C_{10}C_9$) = −177.1°/$\Delta E = 0$ and 3,4-OH-MeNS **8**, ($O_{12}N_{11}C_{10}C_9$) = 17.5°/$\Delta E = 24.1$ kJ mol^{-1}. The negative value of $V_3^{60^\circ}$ is also explained by the stabilising intramolecular H-bond type interactions, which may occur between NO_2 and one of the methyl hydrogen atoms (e.g. conformers 1, 2 or 3, $O_{12}\cdots H(C_{20})$ ca. 236 pm, Fig. 3). The energy barrier for this internal rotation process—from ($O_{12}C_{11}C_{10}C_9$) = 90 to 180°—was calculated to be 31.8 kJ mol^{-1}.

The internal rotation of the 3,4-OH-MeNS methyl group, in turn, is associated to a variation of dihedral ($H_{22}C_{20}C_{10}C_9$), which was studied for the most stable geometry of the molecule (*E* configuration, with ($H_{17}O_8C_5C_4$)/($H_{18}O_7C_6C_5$) = 0°). The best fitting of the experimental data was obtaining by using a combination of both cosine and sine terms—$V_6^{30^\circ} = -0.7$ kJ mol^{-1}, $V'^{60^\circ}_3 = 0.8$ kJ mol^{-1} and $V'^{30^\circ}_6 = 1.1$ kJ mol^{-1} (Fig. 6)—a maximum being obtained for ($H_{22}C_{20}C_{10}C_9$) = 15°, and three minima occurring for ($H_{22}C_{20}C_{10}C_9$) = 105 (the most favoured geometry), 30 and 90°. This conformational behaviour is a consequence of the balance between the stabilising (C_{20})H$\cdots$O(N_{11}) intramolecular hydrogen-type interactions and the energetically unfavoured (C_{20})H$\cdots H_{15}$ steric hindrances (Table 3).

The orientation of the carbon side chain relative to the aromatic ring is defined by the dihedral angle ($C_{10}C_9C_3C_4$). Once more, the values of the Fourier components of the corresponding potential-energy variation reflect a clear preference for planarity—a minimum occurs for ($C_{10}C_9C_3$

Table 2
Relative energies and optimised geometries for the most stable conformers of 3,4-dihydroxy-β-methyl-β-nitrostyrene (3,4-OH-MeNS) (B3LYP/6-31G** level of calculation)

ΔE (kJ mol^{-1})/μ(D)[a]	3,4-OH-MeNS **1** 0.0/5.1	3,4-OH-MeNS **2** 0.6/5.7	3,4-OH-MeNS **3** 1.5/7.3
Bond lengths (pm)			
C_1-C_2[b]	139.2	139.3	139.1
C_2-C_3	140.8	140.7	140.8
C_3-C_4	141.4	141.1	141.3
C_4-C_5	138.3	138.8	138.5
C_5-C_6	140.9	140.8	140.9
C_6-C_1	139.3	139.3	139.3
C_3-C_9	145.8	146.0	145.7
C_9-C_{10}	134.9	134.8	134.9
$C_{10}-C_{20}$	149.6	149.6	149.6
C_5-O_8	137.4	136.0	137.4
C_6-O_7	135.5	137.1	135.5
$C_{10}-N_{11}$	148.0	148.1	147.8
$N_{11}-O_{12}$	123.4	123.4	123.4
$N_{11}-O_{13}$	123.4	123.4	123.5
O_8-H_{17}	96.5	96.9	96.5
O_7-H_{18}	97.0	96.6	97.0
C_1-H_{14}	108.5	108.7	108.4
C_2-H_{15}	108.2	108.5	108.5
C_4-H_{16}	108.8	108.2	108.5
C_9-H_{19}	108.6	108.6	108.6
$C_{20}-H_{21}$	109.1	109.6	109.1
$C_{20}-H_{22}$	109.6	109.1	109.8
$C_{20}-H_{23}$	109.1	109.1	109.1
Bond angles (°)			
$C_2-C_3-C_4$	117.9	117.9	118.4
$C_2-C_3-C_9$	124.8	117.7	117.4
$C_3-C_9-C_{10}$	129.8	130.0	129.7
$C_9-C_{10}-C_{20}$	129.9	129.9	130.1
$C_6-C_5-O_8$	114.6	114.4	120.4
$C_9-C_{10}-N_{11}$	115.6	115.7	115.6
$C_{10}-N_{11}-O_{12}$	119.6	119.6	119.6
$O_{12}-N_{11}-O_{13}$	123.8	123.8	123.8
$C_5-O_8-H_{17}$	110.2	110.3	107.9
$C_{10}-C_9-H_{19}$	114.5	114.6	114.7
$C_{10}-C_{20}-H_{21}$	110.0	110.1	112.0
$C_{10}-C_{20}-H_{22}$	112.1	112.2	110.1
$H_{21}-C_{20}-H_{22}$	109.2	109.0	106.8
$H_{21}-C_{20}-H_{23}$	108.5	108.7	108.6
Dihedral angles (°)			
$C_3-C_4-C_5-C_6$	−1.3	−1.3	0.0
$C_5-C_4-C_3-C_9$	−179.9	−179.7	179.9
$C_4-C_3-C_9-C_{10}$	157.5	−23.4	23.6
$C_3-C_9-C_{10}-C_{20}$	−4.1	−4.6	4.0
$C_3-C_9-C_{10}-N_{11}$	177.4	177.1	−177.5
$C_9-C_{10}-N_{11}-O_{12}$	−177.2	−177.4	177.3
$C_9-C_{10}-N_{11}-O_{13}$	2.3	2.0	−2.2
$C_4-C_5-O_8-H_{17}$	0.4	−0.1	179.6
$C_5-C_6-O_7-H_{18}$	−0.1	0.0	178.5
$C_5-C_6-C_1-H_{14}$	−178.4	179.1	−179.2
$C_6-C_1-C_2-H_{15}$	−177.5	179.6	−179.7
$C_2-C_3-C_4-H_{16}$	−178.8	175.9	−175.9
$C_2-C_3-C_9-H_{19}$	156.7	−20.4	21.5
$C_9-C_{10}-C_{20}-H_{21}$	−21.5	−21.9	−100.3
$C_9-C_{10}-C_{20}-H_{22}$	99.3	99.3	20.6

[a] Total value of energy for the most stable conformer of 3,4-OH-MeNS is −703,925705439 Hartree (1 Hartree = 2625.5001 kJ mol^{-1}); 1D = 1/3 × 10^{-2} cm.

[b] Atoms are numbered according to Fig. 1; the same atom numbering is applicable to all the compounds studied, irrespective of the type of atom.

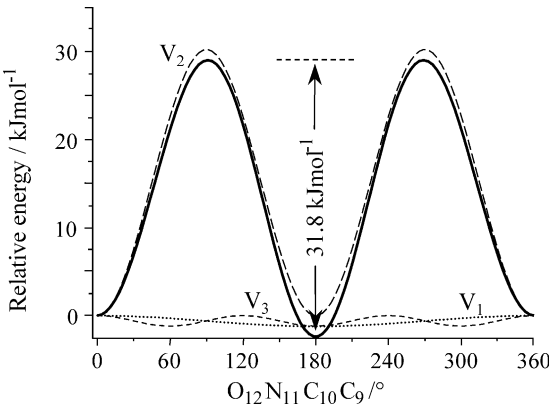

Fig. 5. Optimised conformational energy profile, and its Fourier deconvolution, for the internal rotation around the $N_{11}-C_{10}$ bond of 3,4-OH-MeNS. $V_1 = -1.2$ kJ mol^{-1}, $V_2 = 30.2$ kJ mol^{-1}, $V_3 = -1.2$ kJ mol^{-1} (B3LYP/6-31G* level of calculation).

$C_4) = 150°$ and the cosine term in 90° is by far the primary positive contribution to this profile, $V_2^{90°} = 12.5$ kJ mol^{-1}, as compared to the one in 180°, $V_1^{180°} = -3.1$ kJ mol^{-1} (Fig. 7). This may be attributed to the significant stabilisation due to π-electron delocalisation, which is considerably more effective for a linear *zig-zag* like unsaturated chain, coplanar with the aromatic ring. The fact that the lowest energy conformation was not found to occur for a ($C_{10}C_9C_3C_4$) dihedral equal to 180° is explained by the presence of the methyl group, responsible for (C_{20})H···H_{15} destabilising interactions, which are minimised in the slightly tilted geometry (($C_{10}C_9C_3C_4$) = 150°, (C_{20})H···H_{15} distances of 222 and 275 pm) as compared to the completely planar one (($C_{10}C_9C_3C_4$) = 180°, (C_{20})H···H_{15} distances of 222 pm). A value of 16.5 kJ mol^{-1} was determined for the energy barrier corresponding to this internal rotational process—from ($C_{10}C_9C_3C_4$) equal to 150–90°.

The results presently obtained are in perfect accordance with previously reported data on catechol [29], styrene [30] and β-methylstyrene [31], which were, however, determined by either semi-empirical methods (e.g. AM1), or by

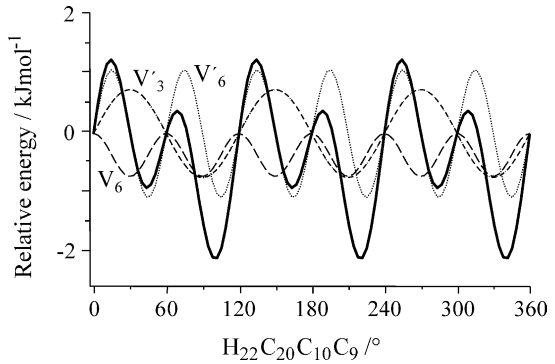

Fig. 6. Optimised conformational energy profile, and its Fourier deconvolution, for the internal rotation around the $C_{20}-C_{10}$ bond of 3,4-OH-MeNS. $V_6 = -0.7$ kJ mol^{-1}, $V'_3 = 0.8$ kJ mol^{-1}, $V'_6 = 1.1$ kJ mol^{-1} (B3LYP/6-31G* level of calculation).

Table 3
Intramolecular $(C_{20})H\cdots H_{15}$ and $(C_{20})H\cdots O(N)$ distances for the distinct geometries yielded by variation of the $(H_{22}C_{20}C_{10}C_9)$ dihedral angle within the 3,4-OH-MeNS molecule (internal rotation of the CH_3 group) (B3LYP/6-31G** level of calculation)

$(H_{22}C_{20}C_{10}C_9)$ (°)	ΔE[a] (kJ mol^{-1})	$d_{(C_{20})H\cdots H_{15}}$[b] (pm)	$d_{(C_{20})H\cdots O(N)}$ (pm)
15	4.38	205	253
30	0.14	218/251	231
45	1.08	220/231	222
60	1.66	221/221	219
75	1.11	219/229	223
90	0.18	218/249	231
99[c]	–	216/266	236
105	0	215/275	240/286
120	1.17	212	250/269

[a] Conformational energies relative to the geometry with $(H_{22}C_{20}C_{10}C_9) = 105°$.
[b] Atoms are numbered according to Fig. 1.
[c] Lowest energy conformer obtained for 3,4-OH-MeNS.

ab initio MO calculations with smaller basis sets than the ones used along this work.

3.2. Raman spectroscopy

Fig. 8 comprises the Raman spectra of the phenolic derivatives studied (in the solid state), in the 75–1750 and 2200–3600 cm^{-1} regions. Harmonic vibrational frequencies were calculated for all conformers of NS, MeNS, 3,4-OH-NS and 3,4-OH-MeNS. A complete assignment of the experimental vibrational features was carried out (Tables 4–6), based on these theoretical calculations, as well as on results previously reported for similar systems [34,35].

Common to all the compounds investigated are the features due to: (i) the NO_2 group—symmetric and asymmetric stretching, at 1250–1336 cm^{-1} and ca. 1550 cm^{-1}, respectively, strong and somewhat weaker absorptions, the latter being often overlapped with the ring C=C stretching; rocking, wagging and scissoring modes, at ca. 500, 700 and 750–800 cm^{-1}, respectively; (ii) the linear chain C=C double bond—stretching vibrations at ca. 1635 cm^{-1}; (iii) the aromatic ring—C=C stretching vibrations, at ca. 1470–1600 cm^{-1}; out-of-plane ring wagging modes—between ca. 870 and 1000 cm^{-1}, for this type of tri-substituted benzenes; (iv) the CH deformations—both wagging, at ca. 1300 cm^{-1}, and rocking modes, at 700–900 cm^{-1}; (v) and the CH typical stretching vibrations, both symmetric and assymmetric, respectively, around 3000–3250 cm^{-1}. While the bands due to the nitro group—around 1300 and 1600 cm^{-1}—are the most intense ones in the spectra of the nitrostyrenes, for the NO_2-free compounds the strongest features are the ones due to the ring wagging modes, at ca. 1000 cm^{-1}.

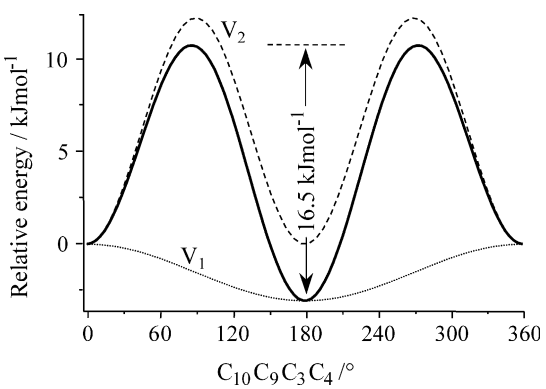

Fig. 7. Optimised conformational energy profile, and its Fourier deconvolution, for the internal rotation around the C_9-C_3 bond of 3,4-OH-MeNS. $V_1 = -3.1$ kJ mol^{-1}, $V_2 = 12.5$ kJ mol^{-1} (B3LYP/6-31G* level of calculation).

Either in the pure liquid or the solid states, phenols usually occur as hydrogen-bonded dimers (and oligomers). Thus, the Raman spectra (in the solid phase) of the hydroxyl-substituted nitrostyrenes—3,4-OH-NS and 3,4-OH-MeNS—comprise the high frequency pattern characteristic of the ring hydroxyl stretching modes: a sharp, moderately intense band at 3520–3400 cm^{-1}—free OH stretch—and a very broad strong absorption near 3300 cm^{-1}—O–H···O stretch (Tables 5 and 6). Also detected are the features at 1315–1400 cm^{-1}, corresponding to the in-plane and out-of-plane C–OH deformations (respectively), and at ca. 1280 cm^{-1}, due to the stretching of the phenol C–O bonds (Tables 5 and 6). In turn, the β-methyl-β-nitrostyrenes—MeNS and 3,4-OH-MeNS—yield the typical CH_3 vibrational bands (Tables 5 and 6): symmetric and antisymmetric stretching modes, between 2800 and 3090 cm^{-1}; symmetric and antisymmetric deformations, at ca. 1320 and 1510 cm^{-1}; rocking modes, around 1000 cm^{-1}; and torsions, at 180–250 cm^{-1}.

It was verified that the presence of the methyl group, responsible for significant inductive effects, as a substituent of the unsaturated carbon chain, led to clear changes in the Raman pattern (Fig. 8, Tables 4–6), namely a clear shift (ca. 20–30 cm^{-1}) of the $\nu(C{=}C)_{chain}$ to higher wavenumbers—S (1634 cm^{-1}) vs. MeS (1663 cm^{-1}), NS (1633 cm^{-1}) vs. MeNS (1654 cm^{-1}), and 3,4-OH-NS (1612 cm^{-1}) vs. 3,4-OH-MeNS (1637 cm^{-1}). Furthermore, in the absence of CH_3 substitution, a large deviation (100–120 cm^{-1}) of the NO_2 scissoring mode to low frequency values is detected—NS (737 cm^{-1}) vs. MeNS (850 cm^{-1}), and 3,4-OH-NS (725 cm^{-1}) vs. 3,4-OH-MeNS (857/867 cm^{-1}). Also, OH substitution of the aromatic ring was found to give rise to low frequency shifts (62–65 cm^{-1}) of the ν_s (NO_2) band, which may be explained by electron delocalisation effects, favoured in the hydroxylated nitrostyrenes—NS (1336 cm^{-1}) vs. 3,4-OH-NS (1279 cm^{-1}), MeNS (1316 cm^{-1}) vs. 3,4-OH-MeNS (1251 cm^{-1}).

The only phenolic aldehyde studied—3,4-OH-BA—exhibits the characteristic $\nu_{C=O}$ band at 1653 cm^{-1} (Table 4). The aldehyde CH is responsible for the feature

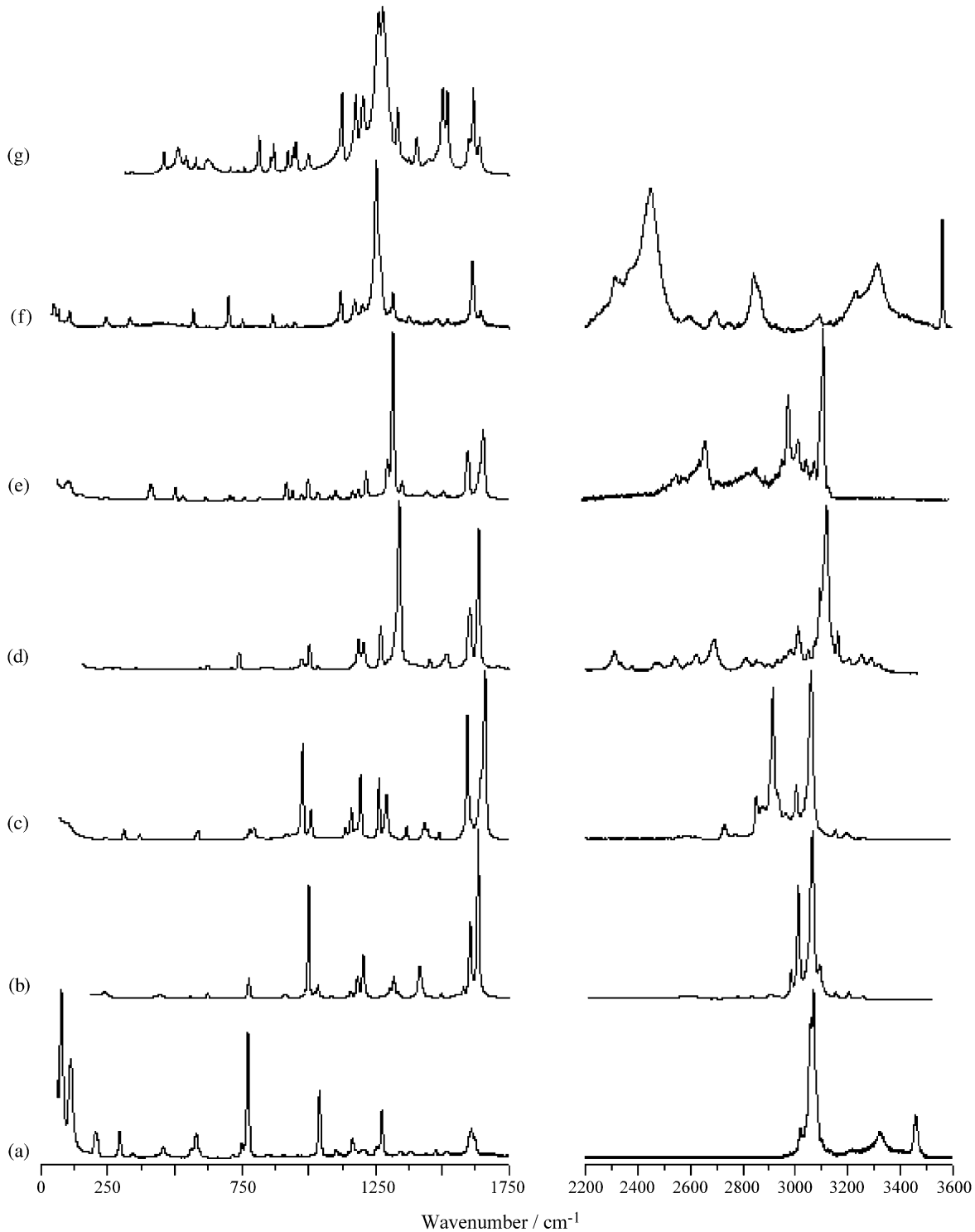

Fig. 8. Experimental Raman spectra (75–1750, 2200–3600 cm^{-1}) of some of the β-nitrostyrene derivatives and their analogues studied in the present work (solid state, at 25 °C): (a) CAT; (b) S; (c) MeS; (d) NS; (e) MeNS; (f) 3,4-OH-MeNS. (g) FTIR spectra (400–1750 cm^{-1}, in KBr pellet) of 3,4-OH-MeNS.

at 1388 cm^{-1}—rocking vibration—as for the characteristic doublet at ca. 2740 and 2890 cm^{-1}, due to a Fermi resonance process between the overtone of that bending mode and the CH stretching fundamental.

The FT-IR spectrum of the β-methyl-β-nitrostyrene of 3,4-OH-MeNS, in the 400–1750 cm^{-1} range, is represented in Fig. 8. The bands due to the stretching modes of the NO_2 group (asymmetric), and the ring and chain double bonds are easily detected, at 1594, 1612 and 1635 cm^{-1}, respectively. Moreover, the bands at ca. 1500 cm^{-1}—CH_3 antisymmetric deformation modes—hardly observed in Raman, appear as well defined, moderately strong features in the FT-IR

Table 4
Raman experimental wavenumbers (cm^{-1}) for CAT, 3,4-OH-BA, S and MeS, in the solid state

Experimental Raman				Approximate description[a]
CAT	3,4-OH-BA	S	MeS	
3459				ν (O_8H_{17})
3324	3326			ν (O_7H_{18})
		3258		ν $(CH)_{ring}$
3211	3181	3203	3195	ν $(CH)_{ring}$
		3154	3155	ν $(CH)_{chain}$
3102	3114	3094 (3080[b])	3101	ν $(CH)_{ring}$
3071				ν $(CH)_{ring}$
3069	3081	3065 (3068[b])	3062	ν $(CH)_{ring}$
3058 (3032[c])	3053	3059	3057	ν $(CH)_{ring}$
		3050 (3050[b])	3046	ν $(CH)_{chain}$
3019		3012 (3030[b])	3004	ν $(CH)_{ring}$
	2980			FR (δ (CH) + ν (CH))
		2984		ν (CH_2)
	2964		2964	ν $(CH)_{ring}$
			2935	ν (CH)
			2916	ν $(CH)_{chain}$
		2909		ν (CH_2)
	2890		2874 (2881[d])	ν_{as} (CH_3)
			2852	ν_s (CH_3)
	1653			ν (C = O)
		1634 (1639[b])	1663 (1668[d])	ν $(C = C)_{chain}$
1621	1645		1647	ν $(CC)_{ring}$
1609 (1625[c])	1592	1604	1599	ν $(CC)_{ring}$
	1582	1578	1579	ν $(CC)_{ring}$
1516	1532	1498 (1499[b])	1495	ν $(CC)_{ring}$
1476	1474			δ $(CH)_{ring}$
	1450	1452 (1432[b])		δ $(CH)_{ring}$ + δ (CH_2) (sciss.)
			1444	δ $(CH)_{ring}$ + δ_{as} (CH_3)
1442	1440			δ $(CH)_{ring}$
	1420	1415		δ $(CH)_{ring}$
1381	1388			δ (CH) + ν (CC)
			1377 (1390[d])	δ_s (CH_3)
1348				δ $(CH)_{ring}$
		1337		ω (CH_2)
		1320		δ_{as} (CH_3)
		1306	1305	δ $(CH)_{chain}$ ν $(CC)_{ring}$
	1292			δ (OH)
1275 (1251[c])	1271			ν CO)
1254			1277	ν $(CC)_{ring}$
		1206	1210	δ $(CH)_{chain}$
1204				ν $(CC)_{ring}$
1177	1188	1184		ν $(CC)_{ring}$
			1177	δ (CH) + δ (OH)
1164	1163			ν $(CC)_{ring}$
1151		1158	1156	ν (CC)
1104	1116			δ $(CH)_{ring}$ + δ (OH)
1041 (1014[c])		1035 (1022[b])	1031	δ $(CH)_{ring}$ + ν $(CC)_{ring}$
		1001 (1003[b])		γ $(CH)_{ring}$ + t (CH_2)
	973		1002	γ $(CH)_{ring}$
			944	γ $(CH)_{ring}$
907		912 (932[b])		ω (CH_2)
846			824	γ $(CH)_{ring}$
	812		809	γ $(CH)_{ring}$
774 (756[c])		777 (771[b])		γ $(CH)_{ring}$
751	755			δ $(CC)_{ring}$
719				δ $(CC)_{ring}$
	628	622	618	δ $(CC)_{ring}$
581	589			δ $(CC)_{ring}$
	502	557 (548[b])		δ $(CC)_{ring}$

(*continued on next page*)

Table 4 (*continued*)

Experimental Raman				Approximate description[a]
CAT	3,4-OH-BA	S	MeS	
457	448	445 (426[b])		δ $(CC)_{ring}$
	426			γ (OH)
			408 (407[d])	γ (CCC)
	406			γ (OH)
	388			γ (OH)
344	362		351	γ (CCC)
296				γ (CCC)
			284	τ (CH_3)
	239	239		δ (CCC)
	222			δ (CCC)
211	214	214		Skeletal modes
206	212			γ (OH)
112	122		132	τ (CH_3)
	104			Skeletal modes
	80			Skeletal modes
77	72			Skeletal modes
	54			Skeletal modes

[a] Atoms are numbered according to Fig. 1; the same atom numbering is applicable to all the compounds studied, irrespective of the type of atom. d and g stand for in-plane and out-of-plane deformations, respectively.
[b] Calculated values [30].
[c] Refs. [29,32,33].
[d] Ref. [31].

Table 5
Raman experimental and calculated wavenumbers (cm^{-1}) for the most stable conformers of NS, MeNS and 3,4-OH-NS, in the solid state

NS		MeNS		3,4-OH-NS		Approximate description[a]
Exp	Calc[b]	Exp	Calc	Exp[c]	Calc	
				3410	3694 (74;123)	ν (O_8H_{17})
				3306	3626 (151;234)	ν (O_7H_{18}) + ν (OH···O)
3231	3144 (7;34)			3117	3144 (8;38)	ν $(CH)_{chain}$
3195	3091 (14;293)		3099 (6;96)	3063	3098 (4;125)	ν_s $(CH)_{ring}$
3153	3083 (23;39)	3070	3086 (24;230)	3040	3082 (4;34)	ν_{as} $(CH)_{ring}$
3111	3076 (7;106)	3057	3076 (15;86)			ν (CH)
3070	3070 (0;65)	3035	3072 (2;60)	2968	3067 (0;38)	ν $(CH)_{chain}$
3046	3067 (0;58)		3067 (0;98)			ν (CH)
3004	3063 (3;10)	2971	3061 (2;18)	2906	3050 (9;45)	ν_{as} $(CH)_{ring}$
2968						
		2936	3041 (4;49)			ν_{as} (CH_3)
		2912	3005 (7;82)			ν_{as} (CH_3)
		2805	2938 (8;160)			ν_s (CH_3)
2666		2619				2 × ν_s (NO_2)
2602						
2524						2 × δ (CH)
2453		2510				
2305						(1000 + 1336) cm^{-1} comb. mode
1633	1639 (130;666)	1654	1652 (53;646)	1612	1636 (108;493)	ν C=C
1600	1593 (15;569)	1596	1593 (4;486)		1600 (104;768)	ν $(CC)_{ring}$
1580	1568 (25;5)		1566 (1;22)	1597	1581 (181;314)	ν $(CC)_{ring}$
1514	1555 (150;151)	1505	1561 (171;49)	1486	1549 (175;263)	ν_{as} (NO_2)
1500	1480 (5;12)	1484	1479 (5;26)	1476	1515 (161;3)	δ $(CH)_{ring}$
			1440 (10;31)			δ_{as} (CH_3)
					1429 (43;5)	ν $(CC)_{ring}$ + δ (OH)
			1433 (14;5)			δ_{as} (CH_3) + δ (CH)
		1443	1427 (7;22)			δ_{as} (CH_3) + δ $(CH)_{ring}$
1450	1433 (15;20)					δ $(CH)_{ring}$ + ν $(CC)_{ring}$

Table 5 (*continued*)

NS		MeNS		3,4-OH-NS		Approximate description[a]
Exp	Calc[b]	Exp	Calc	Exp[c]	Calc	
		1385	1383 (29;16)			δ_s (CH_3) + δ $(CH)_{chain}$
				1328	1373 (27;37)	δ (O_7H_{18})
1395		1349	1335 (18;67)	1313		δ $(CH)_{chain}$ + δ_s (CH_3)
1336	1338 (517;641)	1316	1319 (395;474)	1274	1337 (416;979)	ν_s (NO_2) + δ_s (CH_3)
	1318 (6;18)		1313 (4;11)			δ $(CH)_{ring}$
					1314 (2;31)	δ (CH) + δ (OH)
		1296	1290 (24;109)	1295	1290 (692;530)	δ $(CH)_{ring}$ + ν $(CC)_{ring}$
	1307 (8;9)	1216	1200 (18;145)		1275 (87;3)	δ (CH) + ν $(CC)_{ring}$
	1274 (0;15)			1243	1265 (10;83)	δ $(CH)_{chain}$
1266	1238 (27;224)			1212	1213 (28;79)	δ $(CH)_{chain}$
1203	1182 (14;42)			1199	1176 (209;177)	δ (CH) + δ (O_7H_{18})
1184	1163 (21;91)	1185	1166 (5;39)	1176	1155 (1;4)	δ $(CH)_{ring}$
				1159	1133 (165;59)	δ (O_8H_{17})
	1145 (0;13)	1164	1145 (0;11)			δ $(CH)_{ring}$
1162	1070 (5;1)	1102	1085 (11;19)	1121	1089 (85;2)	δ (CH)
1031	1015 (1;19)	1080	1066 (6;10)			δ $(CH)_{ring}$
		1034	1027 (0;18)			r (CH_3)
	982 (23;5)					
1000	976 (0;42)	999	1017 (0;20)	993	1133 (165;59)	δ $(CH)_{ring}$
				972	975 (26;4)	γ $(CH)_{chain}$
970	965 (3;0)					γ (CH)
	957 (70;37)				963 (104;46)	ν (CN)
			976 (4;52)	931	937 (3;5)	δ $(CC)_{ring}$
	939 (0;0)		967 (1;2)			γ $(CH)_{ring}$
		975	962 (64;8)	922		r (CH_3)
	899 (0;2)	942	942 (3;12)	863	910 (1;1)	γ $(CH)_{ring}$ (as wag)
	838 (1;5)					δ (CC)
		918	932 (15;58)		826 (4;4)	γ $(CH)_{chain}$ + γ $(CH)_{ring}$ (as wag)
	827 (7;8)	870	897 (2;10)	840	806 (50;8)	γ $(CH)_{chain}$ + γ $(CH)_{ring}$ (as wag)
		855	850 (48;4)	828		δ (NO_2) (scis.)
	817 (6;8)	821	826 (0;9)	820	798 (8;5)	γ $(CH)_{ring}$ (as wag)
				812	792 (15;17)	δ $(CC)_{ring}$
		763	804 (8;9)			δ $(CCC)_{chain}$
				779	772 (5;14)	δ $(CC)_{ring}$
	753 (39;2)	720	750 (33;8)			γ $(CH)_{ring}$ (s wag) + γ $(CC)_{ring}$
		707	704 (6;10)		707 (0;0)	ω (NO_2) + γ (CH)
737	720 (12;23)			725	704 (13;35)	δ (NO_2) (sciss.)
		690	689 (12;4)			γ $(CH)_{ring}$ (s wag)
710	693 (10;1)					γ $(CH)_{ring}$ (s wag) + ω (NO_2)
618	667 (14;0)	617	678 (16;4)		667 (0;0)	γ $(CC)_{ring}$
594	609 (0;7)	593	608 (0;7)		580 (23;3)	δ $(CC)_{ring}$
574	585 (20;1)		583 (8;1)	576	566 (8;2)	δ $(CC)_{ring}$
534	481 (7;0)	531	498 (9;18)		575 (6;0)	γ (CC)
515	523 (2;2)	503	521 (7;6)	524	527 (1;5)	r (NO_2) + δ $(CC)_{chain}$
					459 (71;3)	γ (O_7H_{18})
					437 (14;0)	γ (O_7H_{18}) + γ $(CC)_{ring}$
		413	413 (4;16)			γ $(CC)_{chain}$
	396 (0;0)					γ $(CC)_{ring}$
352						
285						
253	346 (0;2)				431 (22;2)	δ (CCC)
			404 (2;6)		384 (3;2)	γ $(CC)_{ring}$
			381 (1;1)			γ (CCC)
					318 (4;1)	δ (COH)
					291 (1;6)	δ (CCC)
185	290 (1;3)	281	331 (1;1)		277 (2;0)	γ (CCC)
132	257 (0;2)	245	284 (1;3)	229	242 (0;1)	δ (CCN)
					226 (154;2)	γ (O_8H_{17})
			246 (2;1)	158	182 (6;4)	Skeletal modes
		149	190 (0;3)			τ (CH_3)

(*continued on next page*)

Table 5 (*continued*)

NS		MeNS		3,4-OH-NS		Approximate description[a]
Exp	Calc[b]	Exp	Calc	Exp[c]	Calc	
		105	118 (1;1)			τ (CH_3)
110	130 (2;1)				136 (3;1)	Skeletal modes
90	109 (2;0)	95	89 (0;5)		93 (3;0)	Skeletal modes
71	90 (1;3)		65 (1;3)		70 (2; 1)	Skeletal modes
	37 (0;0)		40 (0;5)		37 (0;0)	Skeletal modes

[a] Atoms are numbered according to Fig. 1; the same atom numbering is applicable to all the compounds studied, irrespective of the type of atom. d and g stand for in-plane and out-of-plane deformations, respectively.
[b] B3LYP/6-31G** level; wavenumbers above 400 cm^{-1} are scaled by 0.9614 [25] (IR intensities in km mol^{-1}; Raman scattering activities in Å amu^{-1}).
[c] FT-Raman.

Table 6
Raman and IR experimental and calculated wavenumbers (cm^{-1}) for the most stable conformers of 3,4-OH-MeNS, in the solid state

Experimental		Calculated[a]		Approximate description[b]
Raman	IR	3,4-OHMeNS **1**	3,4-OHMeNS **2**	
3521	3518	3693 (72;123)	3690 (117;277)	ν (O_8H_{17})
		3628 (145;222)	3639 (101;95)	ν (O_7H_{18})
3297				ν (OH···O)
3219				ν (OH···O)
		3115 (3;54)	3117 (1;33)	ν $(CH)_{ring}$
3092		3090 (4;106)	3081 (4;107)	ν $(CH)_{ring}$
2939		2934 (10;175)	2935 (9;169)	ν_{as} (CH_3)
2878		3070 (0;39)	3073 (2;15)	ν_s (CH)
2861		3049 (9;46)	3053 (17;118)	ν_{as} (CH)
2729		3041 (3;56)	3042 (3;54)	ν_{as} $(CH_3)^1$ /ν_s $(CH_3)^2$
2636		3004 (8;75)	3006 (7;76)	ν_s $(CH_3)^1$/ν_{as} $(CH_3)^2$
2498				$2 \times \nu_s$ (NO_2)
2429				
2377				$2 \times \delta$ (CH)
1635	1635	1646 (61;620)	1647 (65;747)	ν $(C{=}C)_{chain}$
	1612	1602 (120;303)	1604 (84;865)	ν $(CC)_{ring}$
1606	1594	1580 (165;105)	1581 (46;2)	ν $(CC)_{ring}$
1512	1514	1554 (140;8)	1556 (153;89)	ν_{as} (NO_2) + ν $(CC)_{ring}$
		1514 (1;40)	1499 (188;0)	ν $(CC)_{ring}$
1473	1497	1443 (37;19)	1455 (3;88)	δ_{as} (CH_3)
	1444	1436 (52;5)	1441 (5;41)	δ_{as} (CH_3)
		1425 (41;15)	1432 (15;25)	δ_{as} (CH_3) + ν $(CC)_{ring}$
1398	1400	1382 (15;76)	1385 (25;15)	δ_s (CH_3) + δ $(CH)_{chain}$ + δ (O_7H_{18})
1370	1371	1374 (4;81)	1349 (20;66)	δ (O_8H_{17}) + δ_s $(CH_3)^2$ + ν $(CC)_{ring}$
1343				
1328	1329	1340 (263;739)	1328 (8;67)	δ $(CH)_{chain}$ + δ_s (CH_3) + δ (O_7H_{18})
1315				
1311	1303			
1295				
1266				
1250	1273	1314 (342;482)	1317 (209;514)	ν_s (NO_2) + δ_s (CH_3) + δ $(CH)^1$ + δ $(O_7H_{18})^2$
	1258	1294 (394;118)	1303 (323;308)	δ (OH) + δ $(CH)^1_{ring}$ + ν_s $(NO_2)^2$
		1280 (52;26)	1283 (534;371)	δ $(CH)_{ring}$ + ν $(CO)^1$ + ν $(CC)^1_{ring}$
1172		1261 (198;210)	1240 (26;26)	δ (CH)
		1183 (4;3)	1180 (55;4)	δ (O_7H_{18}) + δ (CH)
1120	1121	1156 (130;32)	1161 (26;137)	δ (CH) + δ (OH)
1102	1102	1135 (100;3)	1135 (41;4)	δ (O_8H_{17}) + δ $(CH)_{ring}$
1037		1093 (22;66)	1097 (214;77)	δ $(CH)_{ring}$ + δ (O_8H_{17})
1001		1082 (1;20)	1078 (2;23)	δ (CH_3) + δ $(CH)_{chain}$
999	998	1026 (38;12)	1026 (0;22)	r (CH_3) + γ $(CH)^1_{chain}$
950	950	977 (58;131)	978 (40;10)	δ (CH) + r (CH_3)
940	940	934 (23;0)	932 (17;82)	γ $(CH)_{chain}$
920	920	919 (29;10)	932 (65;32)	δ (CH) + r (CH_3) + γ $(CH)^1_{chain}$ + δ $(CH)^1_{ring}$ (as wag)

Table 6 (*continued*)

Experimental		Calculated[a]		Approximate description[b]
Raman	IR	3,4-OHMeNS **1**	3,4-OHMeNS **2**	
866	867	914 (51;6)	883 (2;1)	δ $(CH)_{ring}$ (as. wag)
	858	838 (34;2)	853 (25;7)	δ (CCN) + δ (NO_2) (sciss) + r (CH_3) + δ $(CH)^1_{ring}$ (s wag)
	813	821 (10;10)	841 (49;4)	δ $(CH)_{ring}$ (s wag)
		803 (5;15)	784 (22;11)	δ $(CH)_{ring}$ (as wag)
755	758	776 (11;13)	774 (28;9)	δ $(CH)_{ring}$ (s wag) + ν (CO) + ν (CC)
	736	767 (8;1)	740 (4;20)	γ (CC) + δ $(CH)_{ring}$ (s wag) + ν (CO)
723	723	712 (1;31)	712 (6;1)	δ $(NO_2)_{wag}$
706	706	686 (2;1)	690 (3;25)	δ (CH_3) + δ_{as} (CCN) + γ (CC)
	621	668 (12;1)	668 (1;3)	γ (ring) + δ (CH_3)
590	591	594 (19; 4)	596 (10;6)	γ (ring)
576	578	575 (5;8)	572 (1;9)	δ_s (ring)
573	575	561 (3;20)	555 (23;6)	δ (CC)
	542			
532	535	523 (59;2)	512 (11;12)	r (NO_2) + ν (CN)
	512			
	478			
	459	458 (3;20)	464 (9;10)	γ (O_7H_{18}) + δ (CCC)
		448 (59;2)	449 (4;14)	γ (O_7H_{18}) + γ $(CCC)_{chain}$
		435 (34;14)	425 (18;23)	γ (O_7H_{18}) + γ (CCC)
		427 (19;3)	414 (55;2)	γ (CCC)
353		376 (1;15)	376 (1;0)	δ (CH_3)
338		348 (1;0)	346 (2;1)	γ $(CCC)_{ring}$ + δ (CCN)
		304 (4;0)	301 (5;0)	δ (OH) + δ (COH)
252		279 (0;2)	291 (3;1)	δ (CCC) + δ (CH_3) + δ (O_8H_{17})
		244 (10; 4)	269 (71;2)	γ (OH) + τ $(CH_3)^1$
		239 (1;4)	245 (97;4)	τ $(CH_3)^1$ + γ $(O_8H_{17})^2$
		225 (139;2)	222 (7;2)	δ (CH_3) + γ $(O_8H_{17})^1$
		189 (11;2)	175 (0;6)	τ (CH_3)
117		163 (2;3)	167 (0;0)	τ (CH_3)
111		99 (3;1)	97 (1;0)	τ (CH_3)
77		69 (0;3)	68 (0;3)	Skeletal modes
73		59 (3;1)	59 (1;1)	Skeletal modes
58		34 (1;3)	35 (1;3)	Skeletal modes

[a] B3LYP/6-31G** level; wavenumbers above 400 cm^{-1} are scaled by 0.9614 [25] (IR intensities in km mol^{-1}; Raman scattering activities in Å amu^{-1}).
[b] Atoms are numbered according to Fig. 1; the same atom numbering is applicable to all the compounds studied, irrespective of the type of atom. The indices 1 and 2 refer to conformers 3,4-OHMeNS **1** and 3,4-OHMeNS **2**; δ and γ stand for in-plane and out-of-plane deformations, respectively.

spectrum. Also, the signal at 1273 cm^{-1}, assigned to the NO_2 symmetric stretching, is far more intense than in Raman (at 1266 cm^{-1}), as well as the features due to the NO_2 scissoring modes, between 850 and 900 cm^{-1}, which is in complete accordance with the theoretical results (Table 6).

The spectra did not reveal any changes upon aging of the compounds, which were stored in the dark in order to avoid decomposition due to oxidation and/or dimerisation processes. This is contrary to previous observations in analogous phenols containing a carboxylic function instead of a nitro group, which were found to yield different Raman and FTIR patterns upon aging (even in the solid state) [36–38]. In turn, it was evident that similar molecules give rise to rather distinct Raman patterns—according to their small structural differences—which allows them to be easily distinguished by this spectroscopic technique.

A good overall agreement was obtained between the experimental and calculated frequency values (after scaling according to Scott and Radom [25]), as well as between these and data previously obtained by the authors for the carboxylic compounds caffeic acid [34] and THPPE [35]. Moreover, the present results are in conformity with those reported for similar molecules, namely some of the synthetic precursors of the nitrostyrenes under study [29–33,39] and carboxylated phenols [36–38].

4. Conclusions

A complete conformational analysis was carried out for differently substituted β-nitrostyrenes, through Raman spectroscopy coupled to ab initio methods. Several conformers were calculated for β-nitrostyrene (NS), β-methyl-β-nitrostyrene (MeNS), 3,4-dihydroxy-β-nitrostyrene (3,4-OH-NS) and 3,4-dihydroxy-β-methyl-β-nitrostyrene (3,4-OH-MeNS), varying in the orientation of both

the pendant arm ring substituent and the phenolic hydroxyl groups. The conformational preferences of these compounds were found to be mainly determined by electrostatic factors, as well as by the formation of (C)H···O and (O)H···O intramolecular interactions. Consequently, the calculated relative energies indicate a clear preference for a planar geometry, i.e. for the presence of a completely conjugated system, strongly stabilised through π-electron delocalisation. The few deviations from planarity were explained by the occurrence of strong steric hindrance effects in the planar conformations. A quantitative potential-energy analysis of several internal rotation processes within the molecules under study was carried out.

The results gathered along this work are in very good accordance with the ones obtained in a previous study on the analogous compounds 3-(3,4-dihydroxyphenyl)-2- -propenoic acid (caffeic acid) [34] and 3-(3,4,5-trihydroxyphenyl)-2-propenoic acid (THPPE) [35].

This kind of conformational analysis based on both spectroscopic and theoretical methods, yielding information at the molecular level, is becoming more and more important for the elucidation of the structure-activity relationships ruling the properties of compounds of biological interest, mainly when coupled to biochemical activity assessment experiments. Evaluation assays on the anticancer activity of phenolic derivatives—namely the β-nitrostyrenes described in this work—are presently in course in our laboratory [40], the knowledge of the conformational characteristics of such systems being essential for the interpretation of the biological results. In fact, this type of structure-activity studies may help to decide which structural features of a molecule give rise to its activity, thus contributing for the design of compounds with enhanced cytotoxic properties (e.g. new anticancer drugs).

Acknowledgements

RC and MPM thank the Chemistry Department of the University of Aveiro (in the person of Dr Helena Nogueira), where the FT-Raman and FT-IR experiments were carried out. FB and NM acknowledge FCT—Unit I and D *n*° 226/94, and Project POCTI/QCA III (co-financed by the european community fund FEDER)—for financial support. NM is grateful to FCT for a PhD fellowship (PRAXIS XXI/BD/18520/98).

References

[1] A.G.M. Barret, G.G. Graboski, Chem. Rev. 86 (1986) 751.
[2] R.S. Varma, K.P. Naicker, P.J. Liesen, Tetrahedron Lett. 39 (1998) 3977.
[3] C.-F. Yao, W.C. Chen, Y.M. Lin, Tetrahedron Lett. 37 (1996) 6339.
[4] M. Schmidt, K. Eger, Pharmazie 51 (1996) 11.
[5] K. Bailey, D. Legault, Org. Magn. Res. 16 (1981) 47.
[6] L.R. Worthen, H.W. Bond, J. Pharm. Sci. 59 (1970) 1185.
[7] J.H. Kim, J.H. Kim, G.E. Lee, J.E. Lee, I.K. Chung, Mol. Pharmacol. 63 (2003) 1117.
[8] S. Kaap, I. Quentin, D. Tamiru, M. Shaheen, K. Eger, H.J. Steinfelder, Biochem. Pharmacol. 65 (2003) 603.
[9] P. Groupy, A. Fleuriet, M.J. Amiota, J.J. Macheix, J. Agric. Food Chem. 92 (1991) 39.
[10] M.A. Parker, D. Marona-Lewicka, D. Kurrasch, A.T. Shulgin, D.E. Nichols, J. Med. Chem. 41 (1998) 1001.
[11] M.J. Frisch, et al., GAUSSIAN 98, Revision A.9, Gaussian Inc, Pittsburgh PA, 1998.
[12] T.V. Russo, R.L. Martin, P.J. Hay, J. Phys. Chem. 99 (1995) 17085.
[13] A. Ignaczak, J.A.N.F. Gomes, Chem. Phys. Lett. 257 (1996) 609.
[14] F.A. Cotton, X. Feng, J. Am. Chem. Soc. 119 (1997) 7514.
[15] A. Ignaczak, J.A.N.F. Gomes, J. Electroanal. Chem. 420 (1997) 209.
[16] T. Wagener, G. Frenking, Inorg. Chem. 37 (1998) 1805.
[17] F.A. Cotton, X. Feng, J. Am. Chem. Soc. 120 (1998) 3387.
[18] C. Lee, W. Yang, R.G. Parr, Phys. Rev. B37 (1988) 785.
[19] B. Miehlich, A. Savin, H. Stoll, H. Preuss, Chem. Phys. Lett. 157 (1989) 200.
[20] A. Becke, Phys. Rev. A38 (1988) 3098.
[21] A. Becke, J. Chem. Phys. 98 (1993) 5648.
[22] P.C. Hariharan, J.A. Pople, Theor. Chim. Acta 28 (1973) 213.
[23] M.M. Francl, W.J. Pietro, W.J. Hehre, J.S. Binkley, M.S. Gordon, D.J. DeFrees, J.A. Pople, J. Chem. Phys. 77 (1982) 3654.
[24] C. Peng, P.Y. Ayala, H.B. Schlegel, M.J. Frisch, Comp. Chem. 17 (1996) 49.
[25] A.P. Scott, L. Radom, J. Phys. Chem. 100 (1996) 16502.
[26] L. Radom, W.J. Hehre, J.A. Pople, J. Am. Chem. Soc. 94 (1972) 2371.
[27] L.A.E. Batista de Carvalho, A.M. Amorim da Costa, J.J.C. Teixeira-Dias, J. Mol. Struct. (THEOCHEM) 205 (1990) 327.
[28] G.R. Desiraju, T. Steiner, The weak hydrogen bond in structural chemistry and biology, IUCr Monographs on Chystallography-9, Oxford University Press, UK, 1999, and references therein.
[29] F.J. Ramírez, J.T. López Navarrete, Vib. Spec. 4 (1993) 321.
[30] R. Hargitai, P.G. Szalay, G. Pongor, G. Fogarasi, J. Mol. Struct. (THEOCHEM) 306 (1994) 293.
[31] Y. Haas, S. Kendler, E. Zingher, H. Zuckermann, S. Zilberg, J. Chem. Phys. 103 (1995) 37.
[32] S.J. Greaves, W.W. Griffith, Spectrochim. Acta 47A (1991) 133.
[33] M. Gerhards, W. Perl, S. Schumm, U. Henrichs, C. Jacoby, K. Kleinermanns, J. Chem. Phys. 104 (1996) 9362.
[34] E. Besien, M.P.M. Marques, J. Mol. Struct. (THEOCHEM) 625 (2003) 265.
[35] Fiuza, S.M., Gomes, C.A., Milhazes, N., Borges, F., Marques, M.P.M., J. Molec. Struct., in press.
[36] S. Sánchez-Cortés, J.V. García-Ramos, Spectrochim. Acta A55 (1999) 2935.
[37] S. Sánchez-Cortés, J.V. García-Ramos, Appl. Spectrosc. 54 (2000) 230.
[38] S. Sánchez-Cortés, J.V. García-Ramos, J. Colloid Interf. Sci. 231 (2000) 98.
[39] R.E. Clavijo, R. Araya-Maturana, B.K. Cassels, B. Weiss-López, Spectrochim. Acta 50A (1994) 2105.
[40] C.A. Gomes, M.T. Girão da Cruz, J.L. Andrade, N. Milhazes, F. Borges, M.P.M. Marques, J. Med. Chem. 46 (2003) 5395.